# Molecular Structure of Stilbene in the $T_1$ State. Transient Resonance Raman Spectra of Stilbene Isotopomers and Quantum Chemical Calculations

**Frans W. Langkilde† and Robert Wilbrandt***

*Department of Environmental Science and Technology MIL/KER, Risø National Laboratory, DK-4000 Roskilde, Denmark*

**Albert M. Brouwer**

*Laboratory of Organic Chemistry, University of Amsterdam, NL-1018 WS Amsterdam, The Netherlands*

**Fabrizia Negri, Francesco Zerbetto, and Giorgio Orlandi**

*Dipartimento di Chimica G. Ciamician, University of Bologna, I-40126 Bologna, Italy*

*Received: October 14, 1993; In Final Form: December 3, 1993®*

Time-resolved resonance Raman spectra are reported for the lowest excited triplet state of stilbene and three of its isotopomers. The spectra were obtained using a two-laser pump-and-probe arrangement under various experimental conditions. The spectrum of *trans*-stilbene after direct excitation in a glassy medium at low temperature (glycerol at 203 K) is compared with that of *cis*-stilbene under sensitized excitation in solution at room and low temperature. The dependence of resonance Raman spectra on excitation wavelength in both cases is investigated. The observed spectra and isotopic shifts are discussed and interpreted on the basis of quantum chemical molecular orbital calculations. Optimized geometries and vibrational frequencies in the $T_1$ state are calculated by a semiempirical QCFF/PI Hamiltonian and by means of ROHF *ab initio* methods using the 6-31G basis set. $T_1 \rightarrow T_n$ transition energies and moments are calculated using QCFF/PI and CNDO/S methods, and the triplet–triplet transition responsible for the observed $T_1 \rightarrow T_n$ absorption and resonance Raman spectra is identified as the $T_1 \rightarrow T_{10}$ transition. Corresponding resonance Raman intensities are calculated by QCFF/PI. It is concluded that *trans*- and *cis*-stilbene adopt a common equilibrium geometry in the $T_1$ state, with the ethylenic C=C bond of the ground state being weakened to a bond with essentially single-bond character in the $T_1$ state. The observed spectra in the glass are assigned to a planar geometry, implying that a relative minimum is found at a planar *trans* geometry ($C_{2h}$ point group) on the potential energy surface of the $T_1$ state. A number of observed non-totally symmetric vibrational modes are tentatively assigned to combinations of either $a_u$ or $b_g$ modes, deriving their intensities from relatively large frequency changes upon $T_1 \rightarrow T_{10}$ excitation.

## I. Introduction

Stilbene (1,2-diphenylethylene) is widely used as a model in studies of C=C double-bond isomerization. The $E \leftrightarrow Z$ (*trans* ↔ *cis*) photoisomerization of stilbene has been reviewed in detail.[1-5] Structure and dynamics on the stilbene $S_1$ potential energy surface (PES) have been studied in a number of papers.[6-17] The $S_0$ and $S_1$ states of (*E*)- and (*Z*)-stilbene have been studied by Raman and resonance Raman (RR) spectroscopies,[18-26] as have their anion[27-30] and cation[31] radicals. Structure and dynamics on the $T_1$ PES have been studied by time-resolved optical absorption and emission spectroscopy,[32-34] by optically-detected magnetic resonance[35] (in a single crystal at 1.3 K), and recently by time-resolved RR spectroscopy.[36] The spectroscopic triplet energy of the $T_1$ state has been determined as 51.0 kcal/mol for (*E*)-stilbene and 55.5 kcal/mol for (*Z*)-stilbene; the relaxed triplet energy measured by photoacoustic calorimetry is 46.5 kcal/mol for (*E*)-stilbene and 42.0 kcal/mol for (*Z*)-stilbene.[37]

Görner and Schulte-Frohlinde[32,33] studied the $T_1$ state of stilbene by optical absorption methods. At room temperature, a structureless $T_1 \rightarrow T_n$ absorption spectrum, identical for (*E*)- and (*Z*)-stilbene and increasing monotonically from 400 nm down to the experimental limit of 355 nm, was observed only in the presence of a sensitizer. In Ar-saturated methanol solution at 298 K, the triplet lifetime was 62 ns for (*E*)-stilbene and 60 ns for (*Z*)-stilbene. In viscous solvents and glasses at low temperature, a structured $T_1 \rightarrow T_n$ absorption spectrum with a lifetime of ≈10 ms was observed upon direct excitation of (*E*)-stilbene. In glycerol at 235 K, absorption maxima were found at 385, 366, and 350 nm; in ethanol at 98 K, maxima were found at 381, 361, and 343 nm. It was concluded from these studies[33] that for stilbene in the $T_1$ state an equilibrium exists between a planar *trans* (*E*) geometry and a more stable geometry that is twisted by 90° at the central CC bond (*P*, perpendicular),

$$E \underset{k_{-1}}{\overset{k_1}{\rightleftarrows}} P \rightharpoonup Z \qquad (1)$$

The equilibrium was found to be dependent on solvent polarity. On the basis of quenching by azulene, an equilibrium constant $K_1 = k_1/k_{-1}$ of 4.6 in methanol at room temperature was determined. The value of $K_1$ was higher in nonpolar solvents.

Saltiel et al.[38,39] discussed the relative energy of the *E*, *P*, and *Z* geometries of $T_1$ and the energy gap at the *P* geometry between the $T_1$ and $S_0$ PES. According to their view, a minimum on the $T_1$ PES is found only at the *P* geometry, with local maxima at the *E* and *Z* geometries, and the minimum on the $T_1$ PES at 90° twist is below the maximum on the $S_0$ PES at this geometry, i.e., the potential energy surfaces cross.

We have previously reported time-resolved RR spectra of stilbene in the $T_1$ state.[36] Room temperature $T_1$ RR spectra were identical for (*E*)- and (*Z*)-stilbene. This confirmed that a common

* To whom correspondence should be addressed.
† Present address: Astra Hässle AB, S-431 83 Mölndal, Sweden.
® Abstract published in *Advance ACS Abstracts*, February 1, 1994.

0022-3654/94/2098-2254$04.50/0 

**SCHEME 1: Stilbene Isotopomers and Atom Numbering**

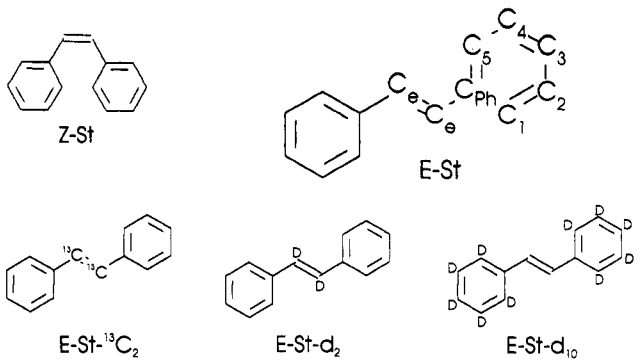


equilibrium distribution of triplet species is reached from either one of the two ground-state isomers. At 203 K and larger viscosity, the $T_1$ RR spectrum of (*E*)-stilbene was qualitatively similar to the room temperature ones, but the RR bands were significantly sharper at 203 K, especially in the frequency region below 1000 $cm^{-1}$. At this temperature, several broad features at low frequencies separated into distinct bands and a strong band appeared at 201 $cm^{-1}$. This band was not observed at 293 K.

The $T_1$ RR spectra were interpreted on the basis of preliminary calculations[36] using a modified version of the semiempirical quantum mechanical consistent force field program (QCFF/PI).[40,41] Under the assumption of a planar *E* structure in the $T_1$ state, most of the observed RR bands were assigned to normal modes of $a_g$ symmetry. However, a number of bands observed at frequencies below 1000 $cm^{-1}$ could not be assigned to $a_g$ fundamentals. These unassigned bands included a RR band of considerable intensity at 459 $cm^{-1}$. The bands were tentatively assigned to overtone or combination modes or to fundamental modes of symmetry other than $a_g$.

To understand more completely the $T_1$ RR spectra of stilbene, and the implications for the molecular structure of the stilbene triplet, we have continued our stilbene studies with respect to both experiment and theory. Experimentally, we have investigated isotopically substituted derivatives of stilbene, and we have obtained triplet RR spectra with different Raman excitation wavelengths and at different temperatures. On the theoretical side, we have performed more extensive quantum chemical calculations. Geometry optimizations and frequency calculations in the $T_1$ state were carried out using the QCFF/PI Hamiltonian on the one hand and *ab initio* ROHF calculations at the 6-31G level on the other. Intensities of the $a_g$ modes (within the $C_{2h}$ point group) were calculated using the QCFF/PI program.

In the present paper we report time-resolved RR spectra, excited at 385 nm in glycerol at 203 K, of the following isotopomers of (*E*)-stilbene: $C_6H_5HCCHC_6H_5$ (*E*-St), $C_6H_5H^{13}C^{13}CHC_6H_5$ (*E*-St-$^{13}C_2$), $C_6H_5DCCDC_6H_5$ (*E*-St-$d_2$), and $C_6D_5HCCHC_6D_5$ (*E*-St-$d_{10}$) (Scheme 1). The spectra are interpreted on the basis of the theoretical calculations. For *E*-St and *E*-St-$^{13}C_2$ in glycerol at 203 K, we report depolarization ratios of RR bands. For (*Z*)-stilbene (*Z*-St) in methanol with benzophenone as sensitizer, we report the $T_1$ RR spectra at 293 and 203 K with 381.2- and 371.2-nm Raman excitation. The molecular structure of stilbene in the $T_1$ state is discussed on the basis of the experimental and theoretical results.

## II. Quantum Chemical Calculations

**A. Methods.** Equilibrium geometries, normal coordinates, and vibrational frequencies were computed by the QCFF/PI program,[40,41] upgraded as described in refs 42 and 43. All singly excited determinants (113) arising from the HOMO–LUMO reference determinant in a space of $5\pi,5\pi^*$ molecular orbitals were included in the CI scheme. Calculations were also performed by the Gaussian 92 series of programs[44] at the ROHF level employing a 6-31G atomic basis set. The vibrational frequencies obtained in this way were scaled by a common factor of 0.9. The semiempirical QCFF/PI model, despite its modest requirement of computational resources, has been shown to be quite reliable in describing conjugated and aromatic systems[45-47] and hence provides an excellent first level of description. The ROHF *ab initio* calculation should provide a good description of the $T_1$ state of stilbene, since this state is essentially a one-configuration state. Electronic energies and wave functions of higher triplet states were computed by the CI procedure outlined above, with both the QCFF/PI and the CNDO/S[48] Hamiltonians. Vibronic interactions and Herzberg–Teller-induced transition moments[49] in the triplet manifold have been calculated according to refs 50 and 51 using the same CI and the CNDO/S Hamiltonian. No attempt has been made to study higher excited triplet states by *ab initio* calculations, since these have not yet been shown to be sufficiently accurate for our purpose. The evaluation of the Franck–Condon integrals is performed by associating to each totally symmetric normal mode a harmonic oscillator due to that particular normal mode in the Raman spectrum. In the absence of normal-mode rotation and frequency variation upon electronic excitation, the displacement parameter, $B_i$, of a given totally symmetric mode furnishes a measure of its Franck–Condon activity. $B_i$ is defined as

$$B_i = 0.172\omega_i^{1/2}(\mathbf{x}_1 - \mathbf{x}_0)\mathbf{M}^{1/2}\mathbf{L}_i \qquad (2)$$

where $\omega_i$ and $\mathbf{L}_i$ are the *i*th vibrational frequency and normal-mode coordinate in the excited state, **M** is the matrix of atomic masses, and $\mathbf{x}_1$, $\mathbf{x}_0$ are the Cartesian coordinate vectors defining the equilibrium structure of the two electronic states involved in the transition. The Franck–Condon intensity for a transition from the vibrationless ground state to the *v*th quantum of the progression is simply given by

$$F_{0v} = \exp(-\gamma)\gamma^v/v! \qquad (3)$$

where

$$\gamma_i = 0.5B_i^2 \qquad (4)$$

**TABLE 1: Structural Parameters of (*E*)- and (*Z*)-Stilbene in the Ground State $S_0$ (Bond Lengths in Å and Angles in deg)[a]**

| *E* isomer | 6-31G[b] | QCFF/PI | exp[c] |
|---|---|---|---|
| $C_e$–$C_e$ | 1.332 | 1.359 | 1.33 |
| $C_e$–$C_{Ph}$ | 1.475 (1.474) | 1.477 | 1.47 |
| $C_{Ph}$–$C_1$ | 1.396 | 1.421 | 1.394 |
| $C_1$–$C_2$ | 1.386 | 1.405 | 1.394 |
| $C_2$–$C_3$ | 1.386 | 1.406 | 1.394 |
| $C_3$–$C_4$ | 1.389 | 1.406 | 1.394 |
| $C_4$–$C_5$ | 1.384 (1.385) | 1.404 | 1.394 |
| $C_5$–$C_{Ph}$ | 1.397 (1.398) | 1.422 | 1.394 |
| $C_eC_eC_{Ph}$ | 126.5 (127.0) | 124.6 | 129 |
| $C_{Ph}C_eC_eC_{Ph}$ | 0.0 | 0.0 | <15 |
| $C_1C_{Ph}C_eC_e$ | 17.2 | 0.0 | 30 |
| ***Z* isomer** | **6-31G** | **QCFF/PI** | **exp[d]** |
| $C_e$–$C_e$ | 1.332 | 1.351 | 1.334 |
| $C_e$–$C_{Ph}$ | 1.482 | 1.483 | 1.489 |
| $C_{Ph}$–$C_1$ | 1.395 | 1.418 | 1.398 |
| $C_1$–$C_2$ | 1.386 | 1.403 | 1.398 |
| $C_2$–$C_3$ | 1.387 | 1.405 | 1.398 |
| $C_3$–$C_4$ | 1.388 | 1.405 | 1.398 |
| $C_4$–$C_5$ | 1.386 | 1.405 | 1.398 |
| $C_5$–$C_{Ph}$ | 1.395 | 1.416 | 1.398 |
| $C_eC_eC_{Ph}$ | 129.6 | 124.0 | 129.5 |
| $C_{Ph}C_eC_eC_{Ph}$ | 5.0 | 9.2 | |
| $C_1C_{Ph}C_eC_e$ | 43.0 | 32.1 | 43 |

[a] For atom numbering see Scheme 1. [b] In parentheses planar optimized geometry. [c] From ref 52. [d] From ref 53.

**TABLE 2: Structural Parameters of (*E*)-, (*Z*)-, and (*P*)-Stilbene in the States $T_1$ and $T_{10}$ (in Parentheses). Bond Lengths Are in Å and Angles in deg[a]**

| | *E* isomer | | *P* isomer | | *Z* isomer | |
|---|---|---|---|---|---|---|
| | 6-31G | QCFF/PI | 6-31G | QCFF/PI | 6-31G[b] | QCFF/PI |
| $C_e$–$C_e$ | 1.514 | 1.466 (1.421) | 1.472 | 1.480 | | 1.476 |
| $C_e$–$C_{Ph}$ | 1.441 | 1.402 (1.433) | 1.459 | 1.407 | | 1.404 |
| $C_{Ph}$–$C_1$ | 1.407 | 1.453 (1.455) | 1.399 | 1.441 | | 1.447 |
| $C_1$–$C_2$ | 1.380 | 1.392 (1.387) | 1.386 | 1.397 | | 1.395 |
| $C_2$–$C_3$ | 1.391 | 1.413 (1.425) | 1.388 | 1.409 | | 1.410 |
| $C_3$–$C_4$ | 1.386 | 1.412 (1.427) | 1.389 | 1.409 | | 1.411 |
| $C_4$–$C_5$ | 1.386 | 1.393 (1.387) | 1.384 | 1.397 | | 1.394 |
| $C_5$–$C_{Ph}$ | 1.403 | 1.452 (1.453) | 1.400 | 1.442 | | 1.447 |
| $C_eC_eC_{Ph}$ | 124.3 | 124.5 (124.3) | 124.8 | 123.6 | | 126.3 |
| $C_{Ph}C_eC_eC_{Ph}$ | 0.0[c] | 0.0 (0.0) | 94.4 | 90.0 | | 52.0 |
| $C_eC_eC_{Ph}C_1$ | 0.0[c] | 0.0 (0.0) | 3.3 | 0.0 | | 5.4 |

[a] For atom numbering see Scheme 1. [b] In the 6-31G calculation the *P* geometry is reached upon optimization since there is no minimum at the *Z* geometry. [c] Planar geometry was imposed.

**TABLE 3: Relative Calculated (CNDO/S and in Parentheses QCFF/PI) $T_1 \rightarrow T_n$ Excitation Energies *E* (eV) and $T_1 \rightarrow T_n$ Oscillator Strengths *f* for the Lowest Triplet States of (*E*)-Stilbene, (*Z*)-Stilbene, and (*P*)-Stilbene (90° Twisted)**

| | (*E*)-stilbene | | | (*Z*)-stilbene | | | (*P*)-stilbene | | |
|---|---|---|---|---|---|---|---|---|---|
| | sym | *E* | *f* | sym | *E* | *f* | sym | *E* | *f* |
| $T_1$ | $B_u$ | 0.000 | | B | 0.000 | | B | 0.000 | |
| $T_2$ | $A_g$ | 2.081 (1.951) | 0.006 (0.003) | A | 2.673 (2.563) | 0.013 (0.007) | A | 3.194 (3.241) | 0.024 (0.001) |
| $T_3$ | $B_u$ | 2.541 (2.360) | | B | 2.881 (2.783) | 0.002 (–) | B | 3.240 (3.241) | 0.002 (–) |
| $T_4$ | $A_g$ | 2.543 (2.359) | 0.004 (–) | A | 2.958 (2.785) | 0.005 (–) | A | 3.242 (3.276) | 0.009 (0.011) |
| $T_5$ | $B_u$ | 2.960 (2.692) | | B | 3.086 (3.001) | 0.003 (0.001) | B | 3.248 (3.295) | 0.004 (0.002) |
| $T_6$ | $B_u$ | 3.180 (2.854) | | B | 3.713 (3.361) | 0.025 (–) | B | 4.315 (4.099) | 0.028 (0.035) |
| $T_7$ | $A_g$ | 3.198 (2.812) | 0.002 (–) | B | 3.772 (3.452) | | A | 4.325 (4.126) | 0.123 (0.164) |
| $T_8$ | $B_u$ | 3.232 (2.954) | | A | 3.792 (3.373) | 0.002 (0.001) | B | 4.393 (4.126) | |
| $T_9$ | $A_g$ | 3.248 (2.978) | 0.040 (0.047) | A | 3.822 (3.436) | 0.066 (0.053) | A | 4.393 (4.126) | |
| $T_{10}$ | $A_g$ | 3.905 (3.696) | 1.193 (1.137) | A | 4.209 (3.971) | 0.490 (0.511) | A | 4.884 (4.862) | 0.528 (0.643) |
| $T_{11}$ | $B_u$ | 3.934 (3.891) | | B | 4.292 (4.195) | – (0.001) | B | 5.224 (5.102) | |
| $T_{12}$ | $A_g$ | 4.230 | | A | 4.516 (4.291) | 0.003 (0.002) | A | 5.226 (5.102) | 0.001 (–) |
| $T_{13}$ | $B_u$ | 4.231 | | B | 4.581 (4.292) | | B | 5.358 (5.180) | |
| $T_{14}$ | $A_g$ | 4.676 | | A | 4.626 (4.537) | 0.002 (0.006) | A | 5.358 (5.181) | – (0.001) |

**B. Results.** In Tables 1 and 2 we report the results of geometry optimization of $S_0$ and $T_1$, respectively. The calculation for the ground state, the geometry of which is well established,[52,53] provides a test for the accuracy of the procedures we have used. From Table 1 it appears that both QCFF/PI and *ab initio* results are in good agreement with the experimental structural parameters; however, QCFF/PI tends to render the stilbene molecule planar in the *trans* isomer, while the *ab initio* calculation leads to a $C_i$ nonplanar minimum, as it is observed experimentally. It was found by *ab initio* methods that the nonplanar $C_i$ form is more stable than the planar form only by a tiny amount (0.03 kcal/mol). In Table 2 we report the structural parameters of the *trans*, twisted, and *cis* isomers in the state $T_1$. No experimental data are available in this case. The CC bond lengths obtained by *ab initio* and the QCFF/PI calculations are similar, and both find the inversion of CC bond lengths in the central moiety of the molecule as the main effect of the $S_0 \rightarrow T_1$ excitation. However, some differences emerge between the two sets of results: (a) while the ring CC bonds are essentially equivalent according to the *ab initio* calculation, the two CC bonds adjacent to the central moiety are longer than the others according to the QCFF/PI method; (b) the central moiety bonds are found longer in the *ab initio* than in the semiempirical calculation; (c) according to the QCFF/PI method minima at the *trans* and *cis* geometries are found, while according to the *ab initio* calculation at the 6-31G level there is only one minimum on the $T_1$ energy surface at the twisted geometry. In Table 3 and Figure 1 we report the energies and the oscillator strengths (*f*) with respect to $T_1$ of the lowest excited triplets at the three most significant geometries. At the *trans* geometry, the lowest triplet state with an appreciable oscillator strength is $T_{10}$, with $f = 1.14$, located at 3.70 eV above $T_1$. Thus, $T_{10}$ represents the state responsible for the intense absorption observed[32,33] at 380 nm, corresponding to 3.26 eV. All the other states in this energy range possess vanishingly small

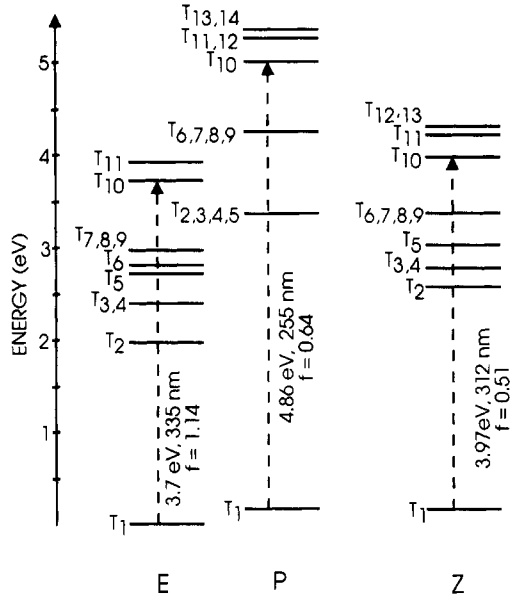


**Figure 1.** Calculated (QCFF/PI) energy levels and transitions of the lowest triplet states of (*E*)-stilbene, (*Z*)-stilbene, and (*P*)-stilbene (twisted by 90° around the central CC bond).

oscillator strengths. A similar result is found for the *cis* geometry. At the twisted geometry two states, $T_7$ and $T_{10}$ have a nonnegligible oscillator strength for the transition to $T_1$. The transition energies of both these states are larger than the transition energy of the active $T_{10}$ state at the *trans* geometry. It follows that the $T_1 \rightarrow T_{10}$ absorption spectrum at the twisted geometry is predicted to be at shorter wavelength than that of the *trans* isomer.

In Table 4 are listed calculated vibrational frequencies, assignments, and $\gamma$-factors (for totally symmetric modes only)

**TABLE 4: Scaled ROHF/6-31G[b] and QCFF/PI[c] Vibrational Frequencies ($cm^{-1}$) and $\gamma$-Factors of the Isotopomers of *trans*-Stilbene *E*-St, *E*-St-$^{13}C_2$, *E*-St-$d_2$, and *E*-St-$d_{10}$ in $T_1$ in the Planar Geometry[a]**

| | *E*-St | | | | *E*-St-$^{13}C_2$ | | | *E*-St-$d_2$ | | | *E*-St-$d_{10}$ | | |
|---|---|---|---|---|---|---|---|---|---|---|---|---|---|
| sym[d] | ROHF, QCFF | assignt[f] | $\gamma$ | obs[e] | ROHF, QCFF | $\gamma$ | obs[e] | ROHF, QCFF | $\gamma$ | obs[e] | ROHF, QCFF | $\gamma$ | obs[e] |
| $a_g$ | 1608, 1580 | $\nu C_{Ph}C_e$ $\nu C_eC_e$ $\phi\nu CC$ | 0.054 | 1573 | 1608, 1568 | 0.015 | 1563 | 1607, 1570 | 0.021 | 1562 | 1564, 1563 | 0.096 | 1557 |
| | 1588, 1532 | $\phi\nu CC$ | 0.103 | 1536 | 1588, 1528 | 0.005 | 1521 | 1587, 1526 | 0.010 | 1521 | 1545, 1507 | 0.045 | 1503 |
| | 1516, 1527 | $\phi\nu CC$ | 0.033 | 1511 | 1508, 1520 | 0.143 | 1505 | 1507, 1514 | 0.168 | 1501 | 1479, 1489 | 0.082 | 1461 |
| | 1482, 1490 | $\phi\nu CC$ | 0.008 | | 1476, 1488 | 0.007 | | 1462, 1477 | 0.001 | 1434 | 1357, 1408 | 0.014 | 1358 |
| | 1441, 1452 | $\phi\nu CC$ | 0.016 | 1425 | 1429, 1443 | 0.027 | 1419 | 1390, 1431 | 0.095 | 1425 | 1318, 1352 | 0.029 | 1318 |
| | 1354, 1397 | $\phi$rCH (CD) | 0.014 | 1341 | 1349, 1394 | 0.023 | 1337 | 1354, 1389 | 0.000 | 1327 | 1079, 1155 | 0.032 | 1095 |
| | 1256, 1313 | $rC_eH$ (CD) | 0.042 | 1243 | 1253, 1311 | 0.041 | 1239 | 1233, 1281 | 0.002 | 1245 | 1222, 1286 | 0.001 | 1280 |
| | 1220, 1269 | $\phi\nu CC$ $rC_eH$ | 0.026 | 1182 | 1217, 1266 | 0.025 | 1180 | 932, 1011 | 0.025 | 958 | 1188, 1255 | 0.039 | 1218 |
| | 1198, 1183 | $\nu C_eC_e$ $\phi$rCH (CD) | 0.008 | | 1198, 1175 | 0.002 | | 1198, 1178 | 0.003 | 1180 | 877, 909 | 0.072 | 869 |
| | 1150, 1164 | $\phi$rCH (CD) | 0.008 | 1110 | 1150, 1161 | 0.007 | 1101 | 1153, 1164 | 0.006 | 1110 | 850, 822 | 0.001 | 829 |
| | 1101, 1143 | $\phi$rCH (CD) $\nu C_eC_e$ | 0.015 | 1067 | 1098, 1133 | 0.026 | 1059 | 1099, 1145 | 0.008 | 1083 | 837, 844 | 0.010 | 855 |
| | 1039, 1075 | $\phi$rCH (CD) | 0.013 | 1050 | 1029, 1070 | 0.021 | 1042 | 1073, 1096 | 0.000 | | 1015, 1061 | 0.022 | 1019 |
| | 1025, 1026 | $\phi$rCH (CD) | 0.024 | 1000 | 1027, 1025 | 0.047 | 999 | 1025, 1026 | 0.021 | 999 | 859, 829 | 0.000 | |
| | 977, 1022 | $\phi\nu CC$ $\delta CCC$ | 0.050 | 966 | 970, 1018 | 0.035 | 963 | 988, 1019 | 0.041 | 978 | 945, 988 | 0.008 | 940 |
| | 846, 899 | $\phi\delta CCC$ $\phi\nu CC$ | 0.037 | 847 | 832, 887 | 0.041 | 837 | 798, 839 | 0.058 | 797 | 787, 793 | 0.003 | 782 |
| | 634, 695 | $\delta CCC$ | 0.005 | 650 | 632, 692 | 0.004 | 651 | 631, 689 | 0.002 | 673 | 610, 671 | 0.004 | 612 |
| | 625, 646 | $\delta CCC$ | 0.000 | 618 | 623, 644 | 0.000 | 616 | 614, 637 | 0.001 | 612 | 602, 627 | 0.000 | 597 |
| | 270, 303 | $\delta CCC$ | 0.014 | 288 | 270, 303 | 0.014 | 288 | 270, 302 | 0.013 | 287 | 255, 285 | 0.013 | 272 |
| | 187, 228 | $\delta CCC$ | 0.038 | 201 | 187, 228 | 0.038 | 198 | 186, 227 | 0.037 | 198 | 179, 219 | 0.041 | 190 |
| $b_u$ | 1605, 1530 | $\phi\nu CC$ | | | 1605, 1530 | | | 1605, 1528 | | | 1561, 1501 | | |
| | 1589, 1528 | $\phi\nu CC$ $\nu C_{Ph}C_e$ | | | 1589, 1527 | | | 1586, 1525 | | | 1543, 1484 | | |
| | 1500, 1488 | $\phi\nu CC$ | | | 1500, 1486 | | | 1500, 1475 | | | 1359, 1417 | | |
| | 1464, 1475 | $\phi\nu CC$ | | | 1463, 1473 | | | 1458, 1466 | | | 1335, 1385 | | |
| | 1362, 1397 | $\phi$rCH (CD) | | | 1361, 1394 | | | 1354, 1378 | | | 1052, 987 | | |
| | 1291, 1354 | $\nu C_{Ph}C_e$ | | | 1285, 1343 | | | 944, 979 | | | 1258, 1319 | | |
| | 1231, 1315 | $rC_eH$ (CD) | | | 1225, 1312 | | | 1232, 1346 | | | 1193, 1267 | | |
| | 1204, 1253 | $\phi\nu CC$ | | | 1204, 1253 | | | 1224, 1276 | | | 877, 841 | | |
| | 1177, 1158 | $\phi$rCH (CD) | | | 1175, 1158 | | | 1192, 1168 | | | 1147, 1237 | | |
| | 1145, 1153 | $\phi$rCH (CD) | | | 1145, 1153 | | | 1150, 1154 | | | 851, 830 | | |
| | 1079, 1087 | $\phi$rCH (CD) | | | 1079, 1086 | | | 1097, 1100 | | | 838, 823 | | |
| | 1027, 1024 | $\phi$rCH (CD) | | | 1027, 1024 | | | 1026, 1028 | | | 1013, 1075 | | |
| | 994, 1018 | $\delta CCC$ $\phi\nu CC$ | | | 994, 1016 | | | 994, 1023 | | | 955, 878 | | |
| | 814, 845 | $\phi\nu CC$ $\delta CCC$ | | | 805, 838 | | | 794, 830 | | | 756, 764 | | |
| | 633, 661 | $\delta CCC$ | | | 632, 661 | | | 632, 660 | | | 607, 639 | | |
| | 544, 580 | $\delta CCC$ | | | 535, 574 | | | 536, 575 | | | 531, 570 | | |
| | 463, 548 | $\delta CC_eC$ | | | 454, 537 | | | 437, 523 | | | 447, 530 | | |
| | 81, 98 | $\delta C_eC_eC$ | | | 81, 97 | | | 81, 97 | | | 76, 92 | | |
| $a_u$ | 1058, 1042 | $\phi$wCH | | | 1058, 1042 | | | 1058, 1042 | | | 901, 833 | | |
| | 1025, 1026 | $\phi$wCH | | | 1025, 1026 | | | 1025, 1026 | | | 839, 826 | | |
| | 951, 914 | $\phi$wCH | | 917 | 951, 914 | | 916 | 951, 914 | | 891 | 796, 805 | | 746 |
| | 871, 831 | $wC_eH$ | | 807 | 871, 828 | | 809 | 871, 817 | | 868 | 680, 737 | | 700 |
| | 784, 810 | $\phi$wCH | | 755 | 784, 808 | | 753 | 784, 744 | | | 649, 638 | | 643 |
| | 708, 738 | $\phi$wCH | | 704 | 708, 708 | | 700 | 708, 646 | | | 551, 625 | | |
| | 499, 634 | $\phi\tau CCC$ | | 602 | 498, 634 | | 596 | 499, 613 | | 561 | 436, 523 | | 503 |
| | 422, 482 | $\phi\tau CCC$ | | 459 | 422, 481 | | 491 | 421, 474 | | 485 | 365, 436 | | 407 |
| | 263, 403 | $\phi\tau CCC$ | | 405 | 257, 403 | | 407 | 253, 402 | | 402 | 252, 361 | | 355 |
| | 108, 233 | $wC_eC_{Ph}$ | | 288 | 108, 230 | | 288 | 104, 226 | | 287 | 100, 221 | | 272 |
| | 25, 60 | $\tau C_{Ph}C_e$ | | | 25, 60 | | | 25, 60 | | | 23, 55 | | |
| | *i*196, 36 | $\tau C_eC_e$ | | | *i*152, 35 | | | *i*196, 35 | | | *i*194, 34 | | |
| $b_g$ | 1058, 1042 | $\phi$wCH | | | 1058, 1042 | | | 1058, 1042 | | | 902, 827 | | |
| | 1026, 1026 | $\phi$wCH | | | 1026, 1026 | | | 1025, 1026 | | | 839, 814 | | |
| | 951, 914 | $\phi$wCH | | 917 | 951, 914 | | 916 | 951, 914 | | 891 | 798, 770 | | |
| | 873, 819 | $\phi$wCH | | 807 | 873, 818 | | 809 | 872, 817 | | 868 | 682, 726 | | |
| | 786, 770 | $wC_eH$ $\phi$wCH | | 755 | 786, 763 | | 753 | 786, 746 | | | 652, 640 | | |
| | 708, 724 | $\phi$wCH $wC_eH$ | | 704 | 708, 721 | | 700 | 708, 658 | | | 550, 610 | | |
| | 511, 625 | $\phi\tau CCC$ | | 602 | 509, 625 | | 596 | 509, 603 | | 561 | 454, 523 | | |
| | 420, 470 | $\phi\tau CCC$ | | 459 | 420, 469 | | 459 | 420, 451 | | 445 | 374, 427 | | |
| | 382, 408 | $\phi\tau CCC$ | | 405 | 379, 408 | | 407 | 329, 408 | | 402 | 361, 367 | | |
| | 228, 306 | $\tau C_eC_{Ph}$ | | 288 | 225, 300 | | 288 | 199, 272 | | 287 | 219, 297 | | |
| | 106, 137 | $\tau C_eC_{Ph}$ | | | 105, 137 | | | 102, 137 | | | 102, 128 | | |

[a] The molecular geometry ($C_{2h}$ point group) for this table corresponds to a stationary point for the QCFF/PI Hamiltonian; for ROHF/6-31G the planarity is imposed, resulting in one imaginary frequency. Assignments of $b_g$ and $a_u$ modes are tentative possibilities; see text. [b] Calculated ROHF/6-31G frequencies $\omega$, $cm^{-1}$; *i* denotes imaginary frequencies. All ROHF frequencies are scaled down by a factor 0.9. [c] Calculated QCFF/PI frequencies $\omega$, $cm^{-1}$ (no scaling of frequencies). [d] Symmetry. [e] Observed frequencies $\omega$, $cm^{-1}$, corresponding to spectra in Figure 2. [f] Potential energy distribution; Ph, $\phi$ = ring, e = ethylenic, $\nu$ = stretch, r = in-plane bend, w = out-of-plane wag, $\delta$ = in-plane skeletal deformation, $\tau$ = out-of-plane skeletal deformation.

for (*E*)-stilbene and its three isotopomers in the $T_1$ state at the planar geometry. As mentioned above, it should be noticed that while the planar geometry is a stationary point according to QCFF/PI, it is a transition state with respect to 6-31G calculations. This is the reason for the imaginary frequencies for the $a_u$ mode of lowest frequency (torsion of the central CC bond). Corresponding calculations were carried out for the *Z* isomer and the twisted form but are not shown here.

## III. Experiment

**A. Materials.** Methanol (Merck, p.a.) and glycerol (Merck, wasserfrei reinst, Art. 4093) were used as received. Benzophenone

(Fluka, purum) was recrystallized from methanol. (*E*)-stilbene (Fluka, purum, for scintillation) was found by gas chromatography (GC) to have an isomeric purity of 99% (GC conditions: DB1 capillary column with He as carrier gas; temperatures: injection (split) 210 °C, column 185 °C, and detection 200 °C). (*Z*)-Stilbene (Aldrich, 97%) was purified by vacuum distillation and found by GC to have an isomeric purity >99.5%.

*E*-St-$^{13}C_2$, a gift from Prof. T. Gustafson, was from MSD isotopes (MS-3026, 99 atom % $^{13}C$). The deuteriated isotopomers of (*E*)-stilbene were synthesized according to known procedures.[54] Benzoic acid was reduced with $LiAlD_4$ to afford benzyl-$d_2$ alcohol. This was oxidized with $BaMnO_4$ to benzaldehyde-$d$.[54] Benzaldehyde-$d_5$ was synthesized by oxidation of benzyl-$d_5$ alcohol (Merck) with pyridinium chlorochromate.[55] Reductive self-coupling of benzaldehyde-$d$ ($d_5$) with low-valent titanium as described by Fürstner et al.[56] yielded a mixture of (*E*)- and (*Z*)-stilbene-$d_2$ ($d_{10}$), in which the *E* isomer was predominant. The crude material was purified by column chromatography ($SiO_2$, eluent ether/petroleum ether 1:5) and crystallization from ethanol. The $^1H$ NMR spectra of the (*E*)-stilbenes thus obtained indicated complete (>95%) deuterium incorporation. For final purification the (*E*)-stilbenes were sublimed *in vacuo* (100–110 deg/15 mm) to yield white crystals.

Solutions containing solvent, (sensitizer), and stilbene were purged with Ar for more than 30 min and transferred to optical cells in a glovebox under Ar, and the cells were closed air-tight with Teflon stoppers.

**B. Methods.** The time-resolved $T_1$ RR spectra were obtained as described before.[36,57] In glycerol at 203 K, the triplet state of the stilbenes was produced by direct excitation with a 308-nm pump pulse from an excimer laser (Lambda Physik EMG 102E); in methanol at 293 and 203 K, the triplet state was obtained by exciting benzophenone as sensitizer with a 351-nm pump pulse from an excimer-pumped dye laser (Lambda Physik EMG 102E + FL3002); the pump energy was ca. 4 mJ per pulse at the sample. The RR probe source was a Nd:YAG pumped dye laser (Quantel), the output of which was mixed with the infrared radiation of the YAG in a nonlinear crystal. Probe wavelengths were as follows: for *E*-St in glycerol, 384.5, 375.0, and 369.0 nm; for *Z*-St in methanol, 381.2 and 371.2 nm; for *E*-St-$^{13}C_2$, *E*-St-$d_2$, and *E*-St-$d_{10}$ in glycerol, 385.2 nm. The probe energy was 1–2 mJ per pulse at the sample. Both lasers were pulsed at 5 Hz with pulse lengths of 10–15 ns. Pump–probe time delays were typically 40 ns for experiments in methanol and 160 ns in glycerol. Individual spectra were averaged over 1000 pulses; the triplet state RR spectra were obtained by subtraction procedures.

The sample was contained in a cylindrical Suprasil cell with 26-mm inner diameter and 6-mm inner height, placed in a spinning copper block in an insulating housing. For experiments at 203 K, the cell was cooled by a flow of cold nitrogen gas and the temperature monitored with a Pt-100 resistance sensor. Scattered Raman light was dispersed in a single grating spectrometer ($f$ = 600 mm, 2400 grooves/mm) and detected with a gated (30 ns) intensified photodiode array (OSMA IR4-700 from Spectroscopy Instruments) with 700 active channels. A polarization scrambler was placed in front of the spectrometer.

For *E*-St and *E*-St-$^{13}C_2$ in glycerol at 203 K, RR depolarization ratios were determined as described by Myers et al.,[58] by recording RR spectra with two alternative linear polarizations of the probe beam. A quartz Rochon prism was placed in the probe beam to ensure pure polarization of the beam. The polarization of the probe beam was rotated by 90° with a $MgF_2$ Soleil-Babinet compensator, placed between the Rochon prism and the sample cell. The depolarization ratio $\rho$ is determined by the relation $\rho = I_y/(2I_x - I_y)$, where $I_x$ is the intensity of a vibrational band obtained with the polarization of the probe beam perpendicular, and $I_y$ the intensity with the probe beam polarization parallel, to the optical axis of the spectrometer.

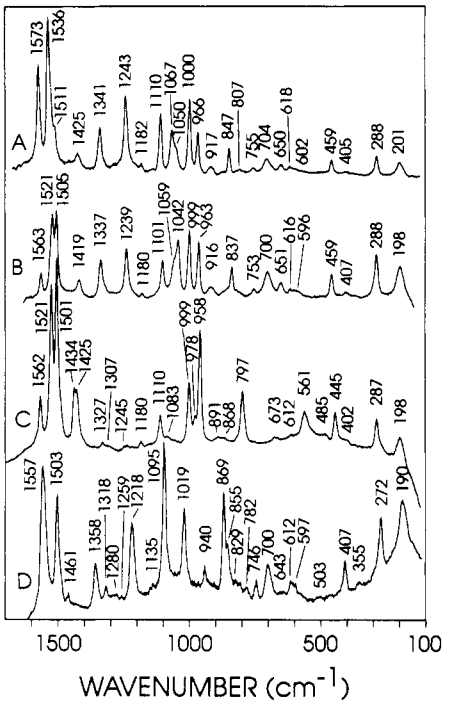


**Figure 2.** Time-resolved resonance Raman (RR) spectra in Ar-saturated glycerol solution at 203 K of the lowest excited triplet state $T_1$ of (A) (*E*)-stilbene, (B) (*E*)-stilbene-$^{13}C_2$, (C) *E*-stilbene-$d_2$, and (D) (*E*)-stilbene-$d_{10}$. For each compound, the spectrum is constructed from three individual spectra from different frequency regions: pump wavelength, 308 nm; probe wavelength (A) 384.5 nm and (B–D) 385.2 nm; pump–probe delay, 160 ns. Bands from solvent and ground-state (*E*)-stilbenes have been subtracted.

Time-resolved absorption measurements were performed using a pulse at 308 nm from an excimer laser as photolyzing light pulse and measuring the transient absorption along a path at right angle to the laser beam. The sample was contained in a cylindrical cell with 2-cm path length mounted in a copper block which was cooled by a flow of cold nitrogen. The analyzing light from a Xe lamp (Varian VIX150UV) passed the cell (active area 2 × 4 mm), was then dispersed in a monochromator (McPherson Model 2035, 0.35-m focal length, grating with 1200 grooves/mm), and detected by a photomultiplier (RCA 1P28). The transient signal was captured and stored in a digital oscilloscope (LeCroy 9450A), and data were handled in a PDP11/23 computer.

**C. Results.** Raman experiments are reported (i) for direct excitation in a glass at low temperature, i.e., in Ar-saturated glycerol solutions of ca. 0.1 mM *E*-St, *E*-St-$^{13}C_2$, *E*-St-$d_2$, and *E*-St-$d_{10}$, and (ii) for sensitized excitation in the liquid state, i.e., for Ar-saturated solutions of 0.034 M *Z*-St in methanol with 0.022 M benzophenone as sensitizer. Subtraction techniques used in the construction of the RR spectra have been discussed in detail previously.[36,57] Each sample cell was used to obtain spectra using (a) the probe laser only and (b) both pump and probe lasers at 40–160 ns time delay between the pump and probe laser pulses. Triplet spectra were obtained from spectra (b) after the subtraction of spectra (a), i.e., bands from solvent, (sensitizer), and ground-state stilbene have been subtracted.

Experimental time-resolved $T_1$ RR spectra, obtained by direct excitation in a glass, i.e., of stilbenes in glycerol at 203 K are shown in Figure 2 for *E*-St (spectrum A), *E*-St-$^{13}C_2$ (B), *E*-St-$d_2$ (C), and *E*-St-$d_{10}$ (D). For each compound, the spectrum is constructed from individual spectra from different frequency regions (≈1650–1050, 1250–650 and 800–150 cm$^{-1}$). The frequencies of the bands in Figure 2 are listed in Table 4 together with the most likely assignments to calculated frequencies (see discussion below). The depolarization ratios $\rho$ of the RR bands were determined for *E*-St in the region 800–150 cm$^{-1}$ and for

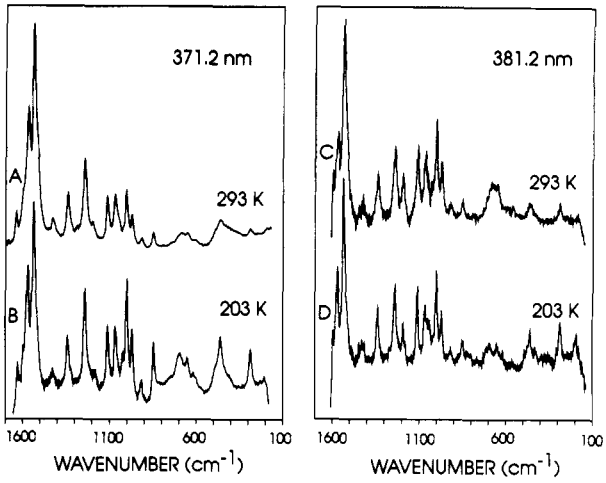


**Figure 3.** Time-resolved resonance Raman (RR) spectra in Ar-saturated methanol solution of 0.034 M (*Z*)-stilbene and 0.022 M benzophenone, of the lowest excited triplet state $T_1$ of stilbene: temperature (A, C) 293 K and (B, D) 203 K; pump wavelength, 351 nm; probe wavelength, (A, B) 371.2 nm and (C, D) 381.2 nm; pump–probe delay, 40 ns. Bands from solvent, sensitizer, and ground-state (*Z*)-stilbene have been subtracted.

*E*-St-$^{13}C_2$ in the region 1650–150 $cm^{-1}$. All bands investigated for the two compounds were found to have $\rho$ close to 0.3.

In Figure 3, the effects of temperature and excitation wavelength on $T_1$ RR spectra excited under sensitized conditions in the liquid state are illustrated. Experimental $T_1$ RR spectra of (*Z*)-stilbene in methanol are shown in Figure 3, A (293 K, probe wavelength 371.2 nm), B (203 K, 371.2 nm), C (293 K, 381.2 nm), and D (203 K, 381.2 nm). Again, each spectrum is constructed from three individual spectra from different frequency regions.

The dependence of RR spectra on excitation wavelength was also investigated for *E*-St in glycerol at 203 K: Spectra were recorded with excitation wavelengths of 384.5, 375.0, and 369.0 nm. Unfortunately, with decreasing excitation wavelength one approaches the ground-state absorption of *E*-St, and fluorescence is induced by the probe pulse. This limited the region of observation to >200 $cm^{-1}$ for 375.0-nm excitation and to >600 $cm^{-1}$ for 369.0-nm excitation. Changes in relative band intensities, but no changes in frequencies or new RR bands were detected in these spectra. The resulting spectra are not shown here.

## IV. Discussion

In a discussion of the multidimensional potential energy surface of the excited triplet state of stilbene, the shape of the surface along torsional coordinates of the ethylenic C=C and the C–phenyl bonds is of particular interest, because these are the main coordinates in the *cis* ↔ *trans* photoisomerization. As mentioned in the Introduction, it is well established that only at high viscosity, e.g., in glasses at low temperature, and only for (*E*)-stilbene, direct excitation leads to considerable population of the lowest triplet state. This has been explained by a shallow minimum at the planar *E* geometry on the PES of the $S_1$ state. At high viscosity and low temperatures, the torsional motion is hindered, and efficient intersystem crossing at the planar *E* geometry takes place; with decreasing viscosity and increasing temperature the radiationless deactivation of the $S_1$ state in the singlet manifold becomes sufficiently rapid to quench the intersystem crossing process completely. (For (*Z*)-stilbene, radiationless deactivation apparently prevents intersystem crossing even in glasses at low temperatures.[59]) Subsequent to the $S_1 \rightarrow T_1$ intersystem crossing process, (*E*)-stilbene finds its new equilibrium on the $T_1$ PES. Our present experiments deal with RR spectra obtained in this equilibrium under varying conditions such as temperature and solvent, and the question arises as to what the equilibrium geometry/geometries in the $T_1$ state and the spectroscopic observables are. This question shall be addressed in the following on the basis of our observed RR spectra, with the discussion structured along the following lines: In sections IVA and IVB the assignment between observed and calculated RR spectra will be discussed. This involves calculated frequencies and intensities from the QCFF/PI and frequencies from the *ab initio* calculations. In section IVA we attempt to assign the RR spectra of the four isotopomers, obtained at high viscosity and low temperature, to the planar *E* form in the $T_1$ state. Arguments for and against this assignment will be discussed in detail. Alternatively, in section IVB, a possible assignment to a twisted form shall be discussed. Section IVC deals with depolarization ratios, section IVD with the effect of excitation wavelength, and section IVE with the effect of temperature and viscosity on the observed RR spectra.

**A. Planar *E* Form, $C_{2h}$ Symmetry.** The QCFF/PI calculations clearly indicate a planar *E* form to be the most stable in the $T_1$ state. Both the planar *Z* and the centrally perpendicular *P* forms were computed approximately 2.9 kcal/mol higher. Torsion around the C–phenyl bonds resulted in a considerably higher energy. Moreover, the calculated (QCFF/PI and CNDO/S) $T_1 \rightarrow T_n$ transition energies further support the spectroscopic importance of the planar *E* form: The $T_1 \rightarrow T_n$ transition observed in the region 350–390 nm (3.54–3.18 eV) is in reasonable agreement with a transition calculated at 3.7 (QCFF/PI) and 3.9 eV (CNDO/S) with an oscillator strength around 1.1 (both methods) for the planar *E* form, while the corresponding transition for the *P* form is calculated ca. 0.9 eV higher in energy with both methods. Other observations support the existence of a stable planar form in the $T_1$ state as well: The $T_1$ lifetime observed in glasses at low temperature is of the order of tens of milliseconds, the $T_1 \rightarrow T_n$ absorption spectrum shows vibrational fine structure, similar to that of the ground state, and a very low quantum yield of *trans–cis* isomerization (0.001–0.01 in glycerol at –80 °C[32]) is reported. A much shorter lifetime would be expected for a twisted equilibrium geometry, due to the small $S_0 - T_1$ energy gap.

In summary, strong evidence, independent of RR spectra, supports an assignment of the spectroscopically observed $T_1$ state of (*E*)-stilbene in glasses at low temperature to a planar *E* geometry. This is at odds with the results of our ROHF/6-31G *ab initio* calculations which predict a minimum lower by 13 kcal/mol than the planar *E* geometry at a geometry twisted by 90° around the ethylenic C=C bond. However, this theoretical result is at variance also with the small (4.5 kcal/mol) difference between the vertical and relaxed $T_1 \rightarrow S_0$ energy gap reported above.

We shall now discuss the assignment of the experimental $T_1$ RR spectra to the spectra calculated for the planar *E* form of the four isotopomers of (*E*)-stilbene, determining the symmetry and the internal coordinates contribution to the vibrational modes that are active in the RR spectra.

*1. RR Spectra, $a_g$ Modes.* For the Raman excitation wavelength in resonance with a strongly-allowed electronic transition ($T_1 \rightarrow T_{10}$ in the case of $T_1$ (*E*)-stilbene), RR spectra are dominated by Franck–Condon scattering, and the vibrational modes observed with strongest intensity are the totally-symmetric ones. They can gain intensity by changes in equilibrium geometry between the two resonant electronic states involved in the transition or by changes in vibrational frequencies. Changes in geometry usually give the dominant contribution. Hence, we shall first attempt to assign the observed RR bands of $T_1$ stilbene according to calculations of changes in equilibrium geometry between the states $T_1$ and $T_{10}$, projected on the totally-symmetric modes of $T_1$. Relative intensities are expressed through the $\gamma$-factors,[42,43] calculated at the planar $C_{2h}$ symmetry of the molecule in the $T_1$ state.

Theoretical $T_1$ RR spectra are constructed in the spectra A (QCFF/PI) and B (*ab initio*) of Figure 4 for the planar *E* form

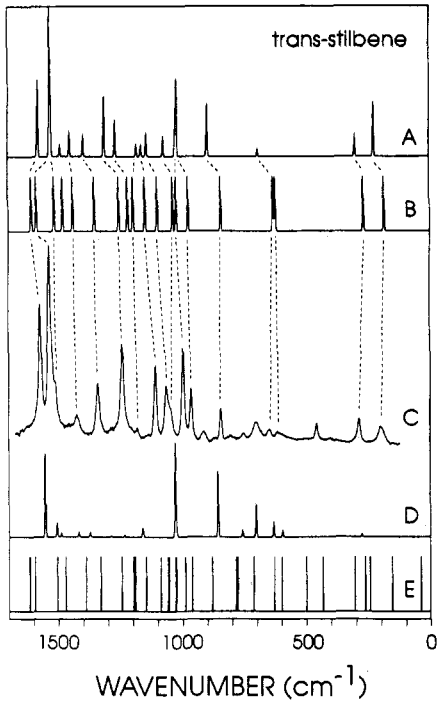


**Figure 4.** Comparison between calculated and experimental resonance Raman spectra of stilbene-$d_0$ in the lowest excited $T_1$ state. (A) Frequencies and intensities ($\gamma$-factors in resonance with the $T_1 \rightarrow T_{10}$ transition) of vibrational modes ($a_g$ symmetry only) in the planar $E$ geometry ($C_{2h}$ point group, stationary point) calculated by QCFF/PI. (B) Frequencies of vibrational modes ($a_g$ symmetry only) in the planar $E$ geometry ($C_{2h}$ point group, imposed geometry, nonstationary point) calculated by ROHF/6-31G level. (C) Experimental RR spectrum (identical to Figure 2A). (D) Frequencies and intensities ($\gamma$-factors in resonance with the $T_1 \rightarrow T_{10}$ transition) of vibrational modes (a symmetry only) of centrally twisted stilbene-$d_0$ ($C_2$ point group, nonstationary point) calculated by QCFF/PI. (E) Frequencies of vibrational modes (a symmetry only) of centrally twisted stilbene-$d_0$ ($C_2$ point group, stationary point) calculated by ROHF/6-31G level.

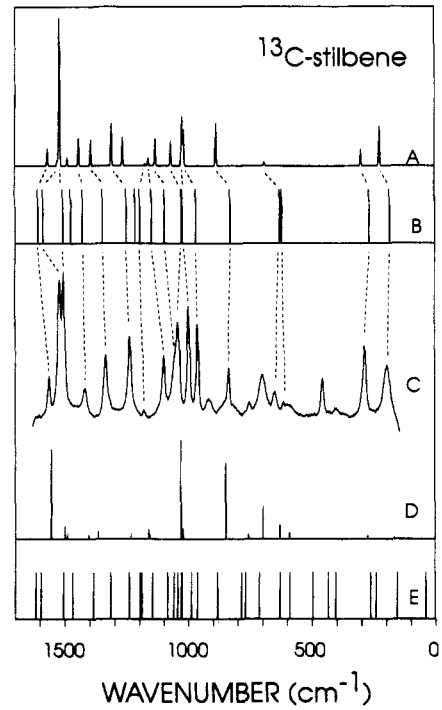


**Figure 5.** Comparison between calculated and experimental resonance Raman spectra of stilbene-$^{13}C_2$ in the lowest excited $T_1$ state. (A) Frequencies and intensities ($\gamma$-factors in resonance with the $T_1 \rightarrow T_{10}$ transition) of vibrational modes ($a_g$ symmetry only) in the planar $E$ geometry ($C_{2h}$ point group, stationary point) calculated by QCFF/PI. (B) Frequencies of vibrational modes ($a_g$ symmetry only) in the planar $E$ geometry ($C_{2h}$ point group, imposed geometry, nonstationary point) calculated by ROHF/6-31G level. (C) Experimental RR spectrum (identical to Figure 2B). (D) Frequencies and intensities ($\gamma$-factors in resonance with the $T_1 \rightarrow T_{10}$ transition) of vibrational modes (a symmetry only) of centrally twisted stilbene-$^{13}C_2$ ($C_2$ point group, nonstationary point) calculated by QCFF/PI. (E) Frequencies of vibrational modes (a symmetry only) of centrally twisted stilbene-$^{13}C_2$ ($C_2$ point group, stationary point) calculated by ROHF/6-31G level.

of $E$-St on the basis of frequencies (QCFF/PI and *ab initio*) and $\gamma$-factors (QCFF/PI) calculated for totally-symmetric vibrational modes. Similar data are shown for the three isotopomers in Figures 5–7. In each figure, the theoretical spectra are compared with the observed one from Figure 2. It should be noticed that the frequencies from *ab initio* calculations for the planar $E$ form (spectra B in Figures 4–7) are not obtained at a stationary point on the PES, but at an imposed planar geometry resulting in one imaginary frequency (ethylenic torsion). In general, the agreement between theory and experiment is satisfactory, and an assignment between the theoretical and observed $T_1$ RR spectra is reasonable for bands with strong or medium intensity in Figures 4–7. In Table 4 we list the observed frequencies for the $T_1$ state of the four isotopomers, together with the calculated (QCFF/PI and *ab initio*) frequencies of $a_g$, $b_g$, and $a_u$ symmetry modes that we assign to the observed bands. We shall now discuss the assignment in some detail.

In our first report on the $T_1$ RR spectrum of $E$-St, we assigned most of the observed bands to $a_g$ normal modes of the planar $E$ structure.[36] This assignment is in agreement with the results from QCFF/PI calculations in the present, more extensive, study. The assignment of observed bands of $E$-St-$^{13}C_2$ (Figure 2B) to calculated $a_g$ normal modes (Figure 5) is very close to that of $E$-St; the calculated and observed isotopic frequency shifts from $E$-St to $E$-St-$^{13}C_2$ are small but consistent. It is evident that replacement of the central carbon atoms by $^{13}C$ does not alter the vibrations in $T_1$ stilbene much. Most $a_g$ modes calculated for $E$-St and $E$-St-$^{13}C_2$ are observed in experiment. Exceptions are the ones calculated (QCFF/PI values) at 1490 and 1183 cm$^{-1}$ for $E$-St (1488 and 1175 cm$^{-1}$ for $E$-St-$^{13}C_2$).

The vibrational pattern is changed more by deuteriation, for both $d_2$ (Figure 2C) and $d_{10}$ substitution (Figure 2D). Again, the observed isitopic shifts are reproduced well by calculation. For $E$-St-$d_2$ (Figure 6) and $E$-St-$d_{10}$ (Figure 7), all calculated $a_g$ bands are found in the experimental spectra, except for those calculated with zero intensity for $E$-St-$d_2$ at 1096 cm$^{-1}$ and for $E$-St-$d_{10}$ at 829 cm$^{-1}$ (QCFF/PI).

*2. RR Spectra, $b_u$, $b_g$, and $a_u$ Modes.* For strictly planar $E$-St with $C_{2h}$ symmetry, in the Franck–Condon approximation, *i.e.*, in the absence of vibronic coupling, only $a_g$ modes are RR-active. Modes of $b_u$, $b_g$, or $a_u$ symmetry can be observed only as either combinations or overtones, containing an even number of vibrational quanta. They derive their intensity from changes in frequency of the normal mode between the two resonant electronic states.[60] As shall be seen below, the positions of most of the observed bands not assigned to $a_g$ modes are close to calculated $b_g$ or $a_u$ modes, and their assignment as overtones seems therefore unlikely. However, it should also be noticed that torsional modes of very low frequency are calculated in the present work, and a fundamental frequency as low as 8 cm$^{-1}$ has previously, in free jet experiments on ground-state stilbene, been observed to be very active and anharmonic and of very large amplitude.[61] Hence, the observed non-totally symmetric vibrations may well be due to combinations of $b_g$ or $a_u$ modes involving low-frequency torsional modes.

Fundamentals of non-totally symmetric modes are in the $C_{2h}$ point group forbidden for modes of ungerade symmetry. Modes of $b_g$ symmetry can gain intensity only due to vibronic coupling between electronic states. If an electronic state $T_m$ is close in energy to the lower state $T_1$ or the upper state $T_n$ in the dominant

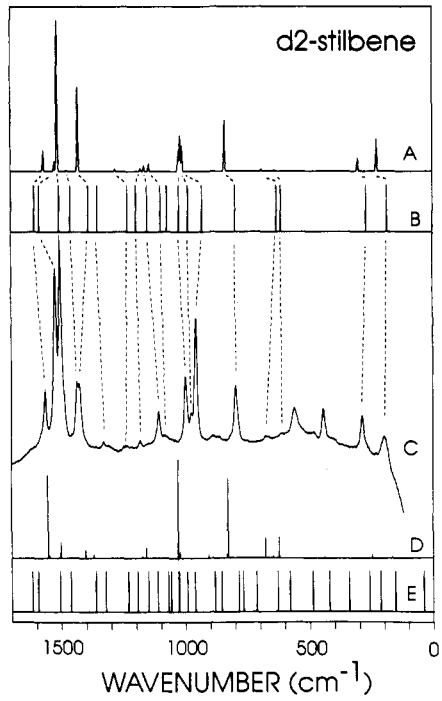


**Figure 6.** Comparison between calculated and experimental resonance Raman spectra of stilbene-$d_2$ in the lowest excited $T_1$ state. (A) Frequencies and intensities ($\gamma$-factors in resonance with the $T_1 \rightarrow T_{10}$ transition) of vibrational modes ($a_g$ symmetry only) in the planar $E$ geometry ($C_{2h}$ point group, stationary point) calculated by QCFF/PI. (B) Frequencies of vibrational modes ($a_g$ symmetry only) in the planar $E$ geometry ($C_{2h}$ point group, imposed geometry, nonstationary point) calculated by ROHF/6-31G level. (C) Experimental RR spectrum (identical to Figure 2C). (D) Frequencies and intensities ($\gamma$-factors in resonance with the $T_1 \rightarrow T_{10}$ transition) of vibrational modes (a symmetry only) of centrally twisted stilbene-$d_2$ ($C_2$ point group, nonstationary point) calculated by QCFF/PI. (E) Frequencies of vibrational modes (a symmetry only) of centrally twisted stilbene-$d_2$ ($C_2$ point group, stationary point) calculated by ROHF/6-31G level.

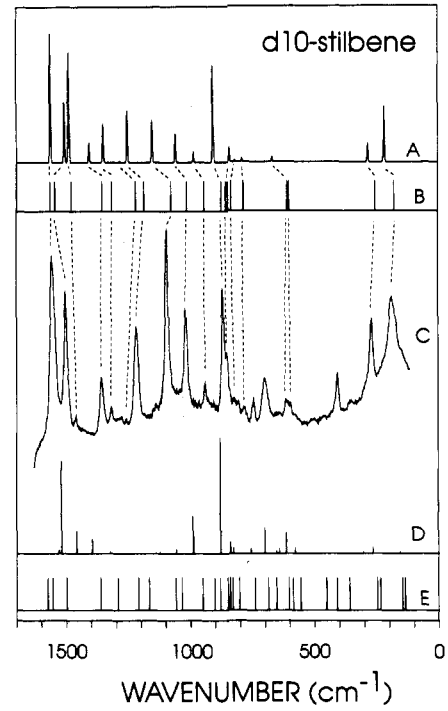


**Figure 7.** Comparison between calculated and experimental resonance Raman spectra of stilbene-$d_{10}$ in the lowest excited $T_1$ state. (A) Frequencies and intensities ($\gamma$-factors in resonance with the $T_1 \rightarrow T_{10}$ transition) of vibrational modes ($a_g$ symmetry only) in the planar $E$ geometry ($C_{2h}$ point group, stationary point) calculated by QCFF/PI. (B) Frequencies of vibrational modes ($a_g$ symmetry only) in the planar $E$ geometry ($C_{2h}$ point group, imposed geometry, nonstationary point) calculated by ROHF/6-31G level. (C) Experimental RR spectrum (identical to Figure 2D). (D) Frequencies and intensities ($\gamma$-factors in resonance with the $T_1 \rightarrow T_{10}$ transition) of vibrational modes (a symmetry only) of centrally twisted stilbene-$d_{10}$ ($C_2$ point group, nonstationary point) calculated by QCFF/PI. (E) Frequencies of vibrational modes (a symmetry only) of centrally twisted stilbene-$d_{10}$ ($C_2$ point group, stationary point) calculated by ROHF/6-31G level.

$T_1 \rightarrow T_n$ transition, non-totally symmetric modes of proper symmetry may vibronically couple $T_m$ with $T_1$ or $T_n$. We have previously found this mechanism to be active for $b_1$ modes in the ground state $D_0$ of the benzyl radical.[43] The upper state $T_n$, active in the present experiments, has been calculated as the $T_{10}$ $\pi\pi^*$ state at 3.905 eV above the $T_1$ state (CNDO/S). For $b_g$ modes to be vibronically active, they can couple either the $T_{10}$ state of $A_g$ symmetry with a $T_m$ $\sigma\pi^*$ excited state of $B_g$ symmetry or the $T_1$ state of $B_u$ symmetry with a $T_m$ state of $A_u$ symmetry.

Alternatively, $T_1$ or $T_n$ $E$-St may not be strictly planar. For a symmetric torsion at the $C_e$=$C_e$ or $C_e$–phenyl bonds in $T_1$, the molecular symmetry is lowered from $C_{2h}$ to $C_2$ (or $C_i$ which is less likely because of a considerably higher energy, as calculated by means of the QCFF/PI method), and normal modes corresponding to $a_u$ or $b_g$ symmetry in $C_{2h}$ may be observed in the RR spectrum. This case shall be discussed in section IVB.

The bands in Figures 2 and 4–7, which cannot be assigned to $a_g$ modes, are observed below 1100 cm$^{-1}$. Since this is the region where modes of $b_g$ and $a_u$ symmetry are found, it is reasonable to relate an assignment of the remaining bands to normal modes or combinations of these symmetries. Tentative assignments are listed in Table 4 together with a full list of calculated frequencies of $b_u$, $b_g$, and $a_u$ symmetry normal modes. For all isotopomers, the calculated frequencies of $b_g$ and $a_u$ modes are similar for many modes. We choose to concentrate on the $b_g$ modes, but as shall be seen below, an assignment to $a_u$ modes or rather their combinations may be more likely, in view of the calculated $a_u$ modes of very low frequency with substantial frequency shifts upon excitation.

On the basis of calculated frequencies only (not intensities), both QCFF/PI and *ab initio*, it is found that $b_g$ and $a_u$ modes are able to account for most of the yet unassigned bands. There is a remarkable qualitative agreement between calculated frequencies and the observed spectra. Indeed, most of the calculated $b_g$ modes do have counterparts in the spectra. In particular, the prominent band observed at 459 cm$^{-1}$ for $E$-St can only be assigned to the calculated $b_g$ band at 470 cm$^{-1}$ (420 cm$^{-1}$ in *ab initio*) or the $a_u$ band at 482 cm$^{-1}$ (422 cm$^{-1}$). This mode is described as an out-of-plane ring CCCC deformation; it is shifted little for $E$-St-$^{13}C_2$ (obs 459 cm$^{-1}$, calc 469 cm$^{-1}$) and $E$-St-$d_2$ (obs 445 cm$^{-1}$, calc 451 cm$^{-1}$), but very much for $E$-St-$d_{10}$ (obs 407 cm$^{-1}$, calc 427 cm$^{-1}$), which confirms its assignment. Moreover, the relative intensity of the observed 288- and 201-cm$^{-1}$ bands is not predicted correctly from the $a_g$ modes at 303 and 228 cm$^{-1}$ alone, but a contribution to the 288-cm$^{-1}$ band from the calculated 306-cm$^{-1}$ $b_g$ mode is possible. Likewise, the broad band observed at 704 cm$^{-1}$ may very well have contributions from both $a_g$ and $b_g$.

For $E$-St and $E$-St-$^{13}C_2$ all calculated modes of $b_g$ symmetry below 1000 cm$^{-1}$ have counterparts in the spectra, and the calculated $b_g$ modes are able to account for all the remaining observed bands.

For $E$-St and $E$-St-$^{13}C_2$ the highest-frequency $b_g$ and $a_u$ modes are calculated and observed close to 1050 cm$^{-1}$. For $E$-St-$d_{10}$, calculation predicts no $b_g$ or $a_u$ modes above 827 cm$^{-1}$. This large isotopic shift is reproduced in the spectra, where all observed bands above 750 cm$^{-1}$ can be assigned to calculated modes of $a_g$ symmetry. All band observed below 750 cm$^{-1}$, which cannot be assigned to $a_g$ modes, can be assigned to calculated modes of $b_g$ or $a_u$ symmetry, in particular the observed 407-cm$^{-1}$ band mentioned above.

For $E$-St-$d_2$ as well, the remaining observed bands can be assigned to calculated modes of $b_g$ symmetry, except for the band

observed at 485 $cm^{-1}$ and assigned to $a_u$ symmetry. The relatively strong band observed at 561 $cm^{-1}$ is assigned to the calculated $b_g$ band at 603 $cm^{-1}$.

In summary, on the basis of calculated frequencies in $T_1$, an assignment of modes which are not of $a_g$ parentage to $b_g$ and $a_u$ modes seems most likely. What then is the mechanism of enhancement? We have calculated the relevant vibronic coupling interactions and have not found any indication of strong vibronic coupling within the manifold of $\pi\pi^*$ and $\sigma\pi^*$ excited triplet states, which could explain the observed spectrum. Alternatively, the observed bands which are not due to $a_g$ modes may be assigned to combinations of $a_u$ or $b_g$ modes of total $a_g$ symmetry involving one of the low-frequency modes. These combinations may derive intensity through Fermi resonance with totally symmetric modes. For *E*-St, on the basis of the QCFF/PI calculations, combinations of $a_u$ modes with the $a_u$ band at 36 $cm^{-1}$ ($\tau(C_eC_e)$) yield a possible assignment. In particular, weak bands in the region below 1000 $cm^{-1}$ may include contributions from such combinations. However, in view of the size of the molecule we have not estimated the anharmonic coupling which could give rise to the experimental observations.

In conclusion, essentially all observed RR bands from the four stilbene isotopomers can be assigned to calculated vibrational modes of the planar *E* form of stilbene in the $T_1$ state, the strongest bands to $a_g$ modes, based on Franck–Condon scattering, and weaker bands to $b_g$ or $a_u$ modes or their combinations. These weak bands gain their intensity from vibronic coupling or Fermi resonance.

**B. Twisted *P* Form, $C_2$ Symmetry.** While the combined experimental and semiempirical results seem to strongly indicate a planar triplet geometry of $C_{2h}$ symmetry as discussed in the preceding section, *ab initio* 6-31G calculations result in a rather deep (13 kcal/mol) minimum at a twisted geometry. We therefore consider in the present section the possibility to assign the observed $T_1$ RR spectra to twisted species, albeit, as mentioned above, the long lifetime, the vibrationally structured $T_1 \rightarrow T_n$ absorption spectrum, and the calculated $T_1 \rightarrow T_n$ transition energy of 4.13–4.88 eV are arguments against this assignment.

Considerable oscillator strengths of 0.12–0.16 and 0.53–0.64 are calculated (see Table 3) by means of QCFF/PI and CNDO/S methods at the perpendicular geomtry for two $T_1 \rightarrow T_n$ transitions, $n = 7$ at 4.126 and $n = 10$ at 4.862 eV above $T_1$, respectively. These transitions are weaker than the $T_1 \rightarrow T_n$ transition of planar *E* stilbene by factors of *ca.* 8.5 ($T_1 \rightarrow T_7$) and 2 ($T_1 \rightarrow T_{10}$). Moreover, the used Raman excitation wavelength is significantly off-resonance with either of the two transitions of the twisted form. It should also be noted that the perpendicular form is not a stationary point on the $T_1$ PES calculated by QCFF/PI, as one frequency (ethylenic C=C torsion) is calculated imaginary. The RR spectra calculated by the QCFF/PI Hamiltonian for the stronger of the two transitions ($T_1 \rightarrow T_{10}$) are shown in spectra D of Figures 4–7. Additionally, frequencies calculated by *ab initio* ROHF/6-31G at the perpendicular stationary point on the $T_1$ PES are shown in spectra E of Figures 4–7. Compared with the results for planar $C_{2h}$ stilbene in $T_1$, considerable changes in frequencies and intensities are calculated.

**RR Spectra.** The frequencies of the totally symmetric vibrational modes of *a* symmetry in the twisted stationary geometry, calculated by *ab initio* methods at the ROHF/6-31G level, are shown in spectra E of Figures 4–7. The calculated spectra can readily account for all observed Raman bands. The reason for this, as opposed to the case for the planar $C_{2h}$ point group, is that modes of $b_g$ symmetry in $C_{2h}$ transform into *a* symmetry in the $C_2$ point group and may become RR-active. In particular, a reasonable agreement is found in the region below 1000 $cm^{-1}$. However, at present the reliable calculation of RR intensities at the *ab initio* level is difficult. This limits the usefulness of this approach in the interpretation of RR spectra of molecules of the size of stilbene considerably.

For the QCFF/PI calculations, spectra calculated for the $T_1 \rightarrow T_7$ transition (not shown) are in rather strong disagreement with the experimental ones while those for the $T_1 \rightarrow T_{10}$ transition (spectra D in Figures 4–7) which, however, is off-resonance agree somewhat better. However, the overall agreement is far worse than for the planar $C_{2h}$ case. Although all the calculated strong bands for all four isotopomers have experimentally observed counterparts, additional observed bands of medium to strong intensity are calculated to have small intensity by theory. This is the case in particular for bands observed below 500 $cm^{-1}$ in *E*-St, *E*-St-$^{13}C_2$, and *E*-St-$d_{10}$ and those below 600 $cm^{-1}$ in *E*-St-$d_2$. The reason for this could be that these bands do not derive their intensity from changes in geometry but from changes in frequency upon $T_1 \rightarrow T_{10}$ excitation, the spectra D in Figures 4–7 only taking into account geometry changes. However, also some intense bands observed above 800 $cm^{-1}$ are not predicted correctly. In particular, the bands observed in *E*-St at 1573, 1341, 1243, 1110, 1067, and 966 $cm^{-1}$, their analogues in *E*-St-$^{13}C_2$, those observed in *E*-St-$d_2$ at 1562 and 958 $cm^{-1}$, and those observed in *E*-St-$d_{10}$ at 1557, 1218, and 1095 $cm^{-1}$ are not predicted by theory. These are bands for which reasonable agreement was found for the planar *E* form.

On the other hand, a remarkable agreement is seen when comparing experimental (Figures 4–7C) and calculated (Figures 4–7D, QCFF/PI) spectra in the region 500–800 $cm^{-1}$. This may be a coincidence, but some contribution from the twisted form cannot be ruled out completely.

In summary, on the basis of calculated frequencies only, it is not possible to distinguish between planar and twisted forms of stilbene in the $T_1$ state, as the uncertainty in calculated frequencies, no matter which method is used, is large compared with the expected differences in frequency. However, if one accepts the validity of the estimates of intensity by the semiempirical method (QCFF/PI), it becomes clear on the basis of calculated RR spectra that while the twisted form certainly may contribute to the observed spectra, it is not the spectroscopically dominant species. This obviously is in contrast to the relatively deep minimum at the twisted geometry predicted by the *ab initio* calculation. In order to explain these different results, it should be remembered that the present *ab initio* calculations are at the rather crude SCF level of theory; in principle, the calculations can be improved by using a larger basis set and a treatment of electron correlation.

From a comparison of the calculated $T_1$ RR spectra in the planar and twisted geometries (both *ab initio* and semiempirical), it can also be concluded that substantial differences, in both frequencies and relative intensities, of RR band are expected for the two forms. For several vibrational bands, calculated changes in frequency when going from a planar to a twisted form are typically in the range 20–40 $cm^{-1}$. As the largest observed differences in frequency are only about 5 $cm^{-1}$, when comparing RR spectra of (*E*)-stilbene in glasses at low temperature with those of (*Z*)-stilbene in solution at room temperature,[36] we conclude that very similar species with respect to the torsional angle of the ethylenic C=C bond are responsible for the experimentally observed RR spectra under the different conditions. This means that we can rule out that the species observed by resonance Raman in glasses and in solution have substantially different conformation.

**C. Depolarization Ratios.** Above, we assigned the experimental RR bands to both in-plane ($a_g$) and out-of-plane ($b_g$ and $a_u$) vibrations. For a molecule of $C_{2h}$ symmetry, nonresonant Raman band depolarization ratios are $\approx$0.3 for in-plane vibrations ($a_g$) and 0.75 for out-of-plane vibrations ($b_g$). We observe depolarization ratios of $\rho \approx 0.3$ for all observed bands. Hence, in spite of the fact that $b_g$ or $a_u$ modes (in $C_{2h}$ point group) are involved in the observed transitions, no depolarized bands are detected.

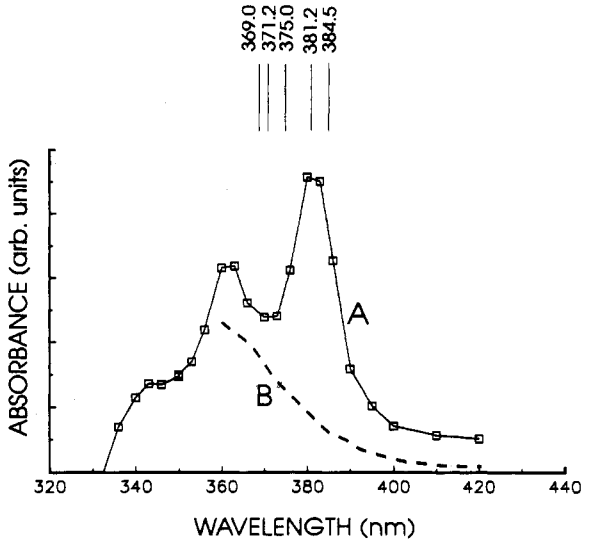


**Figure 8.** $T_1 \rightarrow T_n$ absorption spectra of (*E*) stilbene-$d_0$: (A) $2.2 \times 10^{-5}$ M (*E*)-stilbene-$d_0$ in Ar-saturated glycerol at 202 K, direct excitation at 308 nm (this work). (B) Adapted from ref 33: sensitized (xanthone or benzophenone) excitation of $3 \times 10^{-2}$ M (*E*)-stilbene-$d_0$ in *tert*-butyl alcohol; excitation wavelength, 353 nm; room temperature.

The question of depolarization ratios in RR scattering is a complicated one.[46,62] Myers[62] has recently shown that under a variety of conditions torsional modes can appear as polarized bands in RR scattering. However, our observations with respect to depolarization ratios support the attribution of the non-totally symmetric bands to combination bands resulting in $a_g$ overall symmetry.

**D. Effect of Excitation Wavelength on RR Spectra.** In order to discuss the dependence of the observed RR spectra on exciting wavelength, it is useful to visualize the excitation conditions, as illustrated in Figure 8. We have remeasured the $T_1 \rightarrow T_n$ absorption spectrum of *E*-St in glycerol at 202 K and plotted it (spectrum A) together with the spectrum observed by Görner and Schulte-Frohlinde[33] under sensitized conditions at room temperature in *tert*-butyl alcohol (spectrum B). In glycerol, peaks were observed at 381 and 362 nm, in reasonable agreement with previously published values of 385 and 366 nm. Also indicated in Figure 8 are the various laser excitation wavelengths.

When considering relative intensities in the RR spectra presented in Figures 2–7, it should be mentioned that relative observed intensities are subject to rather large experimental uncertainty. This is due to the fact that (i) the collection optics for Raman light were not achromatic, (ii) no correction was made for the varying sensitivity of the detection system with wavelength, and (iii) no correction was made for reabsorption of the scattered light due to triplet–triplet absorption.

As mentioned above, RR spectra in glycerol were measured with 384.5-, 375.0-, and 369.0-nm excitation (not shown). No frequency changes were observed, and the changes in intensity were rather small. The bands at 1243, 1000, and 917 $cm^{-1}$, and in particular the band at 847 $cm^{-1}$, increased in intensity by approximately a factor 2 relative to the strongest observed band at 1536 $cm^{-1}$ with decreasing excitation wavelength. In general, the observed enhancement pattern reflects the vibrational excess energy of the excitation wavelength with respect to the zero–zero absorption band. In the absence of more complete excitation spectra, no conclusions can be drawn from this.

The wavelength dependence of the $T_1$ RR spectra in the liquid state, i.e., in methanol at two temperatures (293 and 203 K), is shown in Figure 3 for two excitation wavelengths, namely, 381.2 and 371.2 nm. Above 800 $cm^{-1}$, the changes in relative Raman intensities with decreasing excitation wavelength are not dramatic with one notable exception: the band at 1182 $cm^{-1}$ seems considerably more intense with 381.2-nm excitation. Such a large variation in intensity over a relatively limited wavelength range of excitation is usually typical for bands deriving their intensity from vibronic coupling. The change with excitation wavelength of RR spectra due to totally symmetric vibrations has been discussed by several authors.[60,63] Ultimately, it is due to the change in scattering efficiency when the exciting beam frequency moves from resonance with the 0–0 band to the 0–1 or higher bands. Even in the Franck–Condon approximation, i.e., neglecting the contribution of the Herzberg–Teller mechanism, a change in the relative intensity of totally symmetric bands is to be expected,[60] and this depends on the displacement parameter *B* between the initial and the scattering state. The presence of Herzberg–Teller scattering causes interference with the allowed scattering. Such interference is of opposite sign for resonance with the 0–0 and the 0–1 bands,[60,63] giving rise to asymmetric excitation profiles, that is, changes in the shape of RR spectra. This effect has been discussed in detail for the case of weak displacements.[63]

Apart from this, the main observation upon a decrease of excitation wavelength in the liquid phase is an overall increase in resonance Raman intensity, as seen from the increasing signal-to-noise ratio. Below 800 $cm^{-1}$, the data from glycerol glass were incomplete, due to interfering luminescence with decreasing excitation wavelength. For (*Z*)-stilbene in liquid methanol, fluorescence is much weaker or absent, and therefore it was possible to detect RR spectra with shorter excitation wavelength in the low-frequency region. No new bands, overtones or combinations, were detected with the lower excitation wavelength. However, the band at 459 $cm^{-1}$ seems generally broader with 371.2-nm rather than 381.2-nm excitation. Again, in the absence of more detailed excitation spectra, quantitative conclusions are difficult to derive. However, the strong activity of CCCC out-of-plane modes, either as combinations or fundamentals, suggests substantial change in shape of the PES upon $T_1 \rightarrow T_{10}$ excitation.

**E. Effect of Temperature and Viscosity on RR Spectra.** When comparing the RR spectra obtained under various conditions, one has to take into account both the effect of temperature and viscosity. While the viscosity in glycerol at 231 K is very high, $6.7 \times 10^6$ cP,[64] in methanol it ranges from 0.597 cP at 293 K to 4.36 cP at 201 K; for *tert*-butyl alcohol, for which the $T_1 \rightarrow T_n$ absorption spectrum shown in Figure 8 was reported, it is 3.3 cP at 303 K.[64] Hence, viscosity varies by ca. a factor of 7 in the temperature range of the present experiments in the liquid phase and by 6 orders of magnitude for the glycerol glass.

We shall first compare the RR spectra obtained in glycerol at 203 K with 384.5-nm (0–0 band) excitation (Figure 2A) and in methanol at 203 K with 381.2-nm (0–0 band of spectrum in ethanol at 98 K) excitation (Figure 3D). The signal-to-noise ratio is lower in Figure 3D than in Figure 2A, which can be due to a smaller concentration of triplet stilbene or to smaller RR enhancement in Figure 3D. In the latter case, the 0–0 band of the $T_1$–$T_n$ absorption spectrum in methanol at 203 K may not be found at 381 nm. According to the viscosities given above, the absorption spectrum in methanol at 203 K probably is similar to the structureless spectrum in *tert*-butyl alcohol at room temperature. However, apart from the difference in overall intensity, the relative intensities of the bands are similar for Figures 2A and 3D. Only the band at 1182 $cm^{-1}$ is stronger in Figure 3D. It should be noted that the bands at 459, 288, and 201 $cm^{-1}$ are also relatively strong in the methanol 203 K spectrum.

The similarity of the spectra at 203 K in glycerol and methanol indicates that the same stilbene $T_1$ species are created by triplet energy transfer from a sensitizer to ground-state (*Z*)-stilbene and by intramolecular intersystem crossing from $S_1$ to $T_1$ in (*E*)-stilbene. Thus, a very similar state of relaxation of the various internal coordinates is likely to be reached by these two very different mechanisms.

The effect of temperature on the RR spectra in the liquid phase can be seen by comparing spectra A with B and spectra

C with D (Figure 3). For 371.2-nm excitation, all bands below 1000 $cm^{-1}$ increase in intensity with decreasing temperature, while similar, but smaller, changes were observed below 500 $cm^{-1}$ for 381.2-nm excitation wavelength. It is obvious that a similar effect is less pronounced for the bands in the high-frequency region above 1000 $cm^{-1}$. From this it appears that temperature in particular affects the intensity and to some extent bandwidth of low-frequency vibrational modes. Unfortunately, these changes cannot be compared with changes in the absorption spectrum with temperature, as the $T_1 \rightarrow T_n$ absorption spectrum in the liquid phase at 203 K is presently unknown. We do not in detail understand the present results; however, one may think that activity of very low-frequency anharmonic out-of-plane modes which may be active as combinations with other out-of-plane vibrations leads to a decreasing intensity and increasing bandwidth of the observed out-of-plane modes with increasing temperature.

## V. Molecular Structure of $T_1$ Stilbene

Judging from the very different $T_1 \rightarrow T_n$ absorption spectra of stilbene in the glass and in solution (see Figure 8), one may speculate that while the spectrum in glass is typical for a planar aromatic hydrocarbon, that in solution may have a strong contribution from a molecule in a nonplanar geometry in $T_1$. This view is not supported by the resonance Raman measurements reported here. In fact, if this were the case, considerable changes in RR spectra would be expected.

Alternatively, the possibility that both absorption spectra in Figure 8 belong to the same species, but the structured absorption spectrum in the glass belongs to a different transition, not observed in solution because of its weakness, was considered. We extended the absorption measurements in the glass down to 220 nm but did not observe any additional strong absorption band that could be correlated to the one observed in solution.

Hence, we attribute both absorption spectra to the same species. The disappearance of fine structure is due to inhomogeneous broadening, which is particularly strong in the $T_1$ state of stilbene because of the presence of a number of low-frequency modes. The broadening then arises from the population of several levels of such modes in $T_1$ together with frequency changes in these modes between $T_1$ and $T_{10}$. (Frequency changes of up to 15% were calculated for the low-frequency modes.) The torsional mode around the central C–C bond is expected to be particularly active because of a very shallow minimum on the PES along this coordinate. Similar effects are observed also in the $S_0 \rightarrow S_1$ absorption spectrum when the temperature and properties of the solvent are changed.[65]

There is no doubt that the QCFF/PI calculations support an assignment of the observed $T_1$ RR and $T_1 \rightarrow T_n$ absorption spectra in the glass to stilbene in a planar *trans* geometry. The well-resolved absorption spectrum (spectrum A in Figure 8) is typical of aromatic hydrocarbons and cannot be due to the twisted form. The long lifetime of the order of milliseconds of the $T_1$ state in glasses at low temperature is in agreement with this view. This interpretation is also in keeping with the usual picture of a rather flat potential energy surface along the torsional coordinate of the central C=C bond, according to which planar *trans* and centrally twisted geometries are almost degenerate to within 2 kcal/mol, and thus a large population of molecules is in the *trans* form at any temperature. *Ab initio* self-consistent-field calculations suggesting a twisted minimum in the $T_1$ state are in clear contradiction with spectroscopically observed absorption spectra in glasses at low temperature. We conclude that stilbene in low-temperature glasses adopts an essentially planar equilibrium geometry.

For the liquid phase (methanol, 293 and 203 K), optical absorption data[33] were previously interpreted to support an equilibrium between planar and twisted equilibrium forms. On the basis of the present data, as discussed above, we disagree with this view and attribute the transient triplet–triplet absorption spectrum in methanol solutions to the *E* planar form broadened by inhomogeneous line broadening. We suggest that, in the observed wavelength region, the $T_1 \rightarrow T_n$ absorption spectrum is dominated by the planar form while the twisted contributes most at shorter wavelengths, not accessible experimentally, due to strong absorption of ground-state stilbene. It is evident that our excitation wavelengths favors observation of the planar form, and this is the one which is observed as the dominant contribution in the present $T_1$ resonance Raman spectra. In order to observe the twisted form by RR, lower excitation wavelengths would be required.

**Acknowledgment.** We thank Professor T L. Gustafson, University of Ohio, for a sample of *E*-St-$^{13}C_2$, Dr. J. Fenger for help with the lasers, and Dr. K. B. Hansen and E. Engholm Larsen for help with instrumentation and computer software. Furthermore, discussions with Dr. Ole Sonnich Mortensen were very helpful. Grants from the Danish Natural Science Research Council, the Ministero della Pubblica Instruzione of Italy, and NATO (Grant 0137/88) are gratefully acknowledged.

## References and Notes

(1) Saltiel, J.; D'Agostino, J.; Megarity, E. D.; Metts, L.; Neuberger, K. R.; Wrighton, M.; Zafiriou, O. C. In *Organic Photochemistry*; Chapman, O. L., Ed.; Marcel Dekker: New York; 1973; Vol, 3, p 1.
(2) Saltiel, J.; Charlton, J. L. In *Rearrangements in Ground and Excited States*; de Mayo, P., Ed.; Academic Press; New York, 1980; Vol. 3, p 25.
(3) Saltiel, J.; Sun, Y.-P. In *Photochromism: Molecules and Systems*; Dürr, H., Bouas-Laurent, H. Eds.; Elsevier: Amsterdam, 1990; p 64.
(4) Waldeck, D. H. *Chem. Rev.* **1991**, *91*, 415.
(5) Görner, H.; Kuhn, H. J. *Adv. Photochem*, submitted.
(6) Hochstrasser, R. M. *Pure Appl. Chem.* **1980**, *52*, 2683.
(7) Hohlneicher, G.; Dick, B. *J. Photochem.* **1984**, *27*, 215.
(8) Syage, J. A.; Felker, P. M.; Zewail, A. H. *J. Chem. Phys.* **1984**, *81*, 4865.
(9) Syage, J. A.; Felker, P. M.; Zewail, A. H. *J. Chem. Phys.* **1984**, *81*, 4706.
(10) Urano, T.; Hamaguchi, H.; Tasumi, M.; Yamanouchi, K.; Tsuchiya, S.; Gustafson, T. L. *J. Chem. Phys.* **1989**, *91*, 3884.
(11) Schroeder, J.; Schwarzer, D.; Troe, J.; Voss, F. *J. Chem. Phys.* **1990**, *93*, 2393.
(12) Negri, F.; Orlandi, G. *J. Phys. Chem.* **1991**, *95*, 748.
(13) Petek, H.; Fujiwara, Y.; Kim, D.; Yoshihara, K. *J. Am. Chem. Soc.* **1988**, *110*, 6269.
(14) Champagne, B. B.; Pfanstiel, J. F.; Plusquellic, D. F.; Pratt, D. W.; van Herpen, W. M.; Meerts, W. L. *J. Phys. Chem.* **1990**, *94*, 6.
(15) Todd, D. C.; Fleming, G. R. *J. Chem. Phys.* **1993**, *98*, 269.
(16) Sension, R.; Repinec, S. T.; Szarka, A. Z.; Hochstrasser, R. M. *J. Chem. Phys.* **1993**, *98*, 6291.
(17) Lienau, C.; Heikal, A. A.; Zewail, A. H. *Chem. Phys.* **1993**, *175*, 171.
(18) Baranovic, G.; Meic, Z.; Güsten, H.; Mink, J.; Keresztury, G. *J. Phys. Chem.* **1990**, *94*, 2833.
(19) Myers, A. B.; Trulson, M. O.; Mathies, R. A. *J. Chem. Phys.* **1985**, *83*, 5000.
(20) Myers, A. B.; Mathies, R. A. *J. Chem. Phys.* **1984**, *81*, 1552.
(21) Ci, X.; Myers, A. B. *Chem. Phys. Lett.* **1989**, *158*, 263.
(22) Gustafson, T. L.; Roberts, D. M.; Chernoff, D. A. *J. Chem. Phys.* **1984**, *81*, 3438.
(23) Hamaguchi, H.; Urano, T.; Tasumi, M. *Chem. Phys. Lett.* **1984**, *106*, 153.
(24) Iwata, K.; Hamaguchi, H. *Chem. Phys. Lett.* **1992**, *196*, 462.
(25) Phillips, D. L.; Rodier, J.-M.; Myers, A. B. *Chem. Phys.* **1993**, *175*, 1.
(26) Hester, R. E.; Matousek, P.; Moore, J. N.; Parker, A. W.; Toner, W. T.; Towrie, M. *Chem. Phys. Lett.* **1993**, *208*, 471.
(27) Takahashi, C.; Maeda, S. *Chem. Phys. Lett.* **1974**, *28*, 22.
(28) Dosser, L. R.; Pallix, J. B.; Atkinson, G. H.; Wang, H. C.; Levin, G.; Szwarc, M. *Chem. Phys. Lett.* **1979**, *62*, 555.
(29) Hub, W.; Schneider, S.; Dörr, F. *J. Am. Chem. Soc.* **1982**, *104*, 2044.
(30) Hub, W.; Schneider, S.; Dörr, F.; Oxman, J. D.; Lewis, F. D. *J. Am. Chem. Soc.* **1984**, *106*, 708.
(31) Hub, W.; Klüter, U.; Schneider, S.; Dörr, F.; Oxman, J. D.; Lewis, F. D. *J. Phys. Chem.* **1984**, *88*, 2308.
(32) Görner, H.; Schulte-Frohlinde, D. *J. Phys. Chem.* **1979**, *83*, 3107.
(33) Görner, H.; Schulte-Frohlinde, D. *J. Phys. Chem.* **1981**, *85*, 1835.
(34) Görner, H. *J. Phys. Chem.* **1989**, *93*, 1826.
(35) Ikeyama, T.; Azumi, T. *J. Phys. Chem.* **1988**, *92*, 1383.
(36) Langkilde, F. W.; Wilbrandt, R.; Negri, F.; Orlandi, G. *Chem. Phys. Lett.* **1990**, *165*, 66.
(37) Ni, T.; Caldwell, R. A.; Melton, L. A. *J. Am. Chem. Soc.* **1989**, *111*, 457.

(38) Saltiel, J.; Marchand, G. R.; Kirkor-Kaminska, E.; Smothers, W. K.; Mueller, W. B.; Charlton, J. L. *J. Am. Chem. Soc.* **1984**, *106*, 3144.
(39) Saltiel, J.; Ganapathy, S.; Werking, C. *J. Phys. Chem.* **1987**, *91*, 2755.
(40) Warshel, A.; Karplus, M. *J. Am. Chem. Soc.* **1972**, *94*, 5612.
(41) Warshel, A.; Levitt, M. QCPE No. 247. Indiana University, 1974.
(42) Negri, F.; Orlandi, G.; Brouwer, A. M.; Langkilde, F. W.; Wilbrandt, R. *J. Chem. Phys.* **1989**, *90*, 5944.
(43) Langkilde, F. W.; Bajdor, K.; Wilbrandt, R.; Negri, F.; Zerbetto, F.; Orlandi, G. *J. Chem. Phys.*, in press.
(44) Frisch, M. J.; Trucks, G. W.; Head-Gordon, M.; Gill, P. M. W.; Wong, M. W.; Foresman, J. B.; Johnson, B. G.; Schlegel, H. B.; Robb, M. A.; Replogle, E. S.; Gomperts, R.; Andres, J. L.; Raghavachari, K.; Binkley, J. S.; Gonzales, C.; Martin, R. L.; Fox, D. J.; Defrees, D. J.; Baker, J.; Stewart, J. P.; Pople, J. A. *Gaussian 92*; Gaussian, Inc.: Pittsburgh, PA, 1992.
(45) Warshel, A. In *Modern Theoretical Chemistry*; Segal, A., Ed.; Plenum Press: New York, 1977; Vol. 7, Part A, p 133.
(46) Hemley, R. J.; Brooks, B. R.; Karplus, M. *J. Chem. Phys.* **1986**, *85*, 6550.
(47) Orlandi, G.; Zerbetto, F.; Zgierski, M. Z. *Chem. Rev.* **1991**, *91*, 867.
(48) Del Bene, J.; Jaffé, H. H. *J. Chem. Phys.* **1968**, *48*, 1807.
(49) Herzberg, G.; Teller, E. *Z. Phys. Chem. (Munich)* **1933**, *B21*, 410.
(50) Orlandi, G. *Chem. Phys. Lett.* **1976**, *44*, 277.
(51) Orlandi, G.; Marconi, G. *Chem. Phys. Lett.* **1978**, *53*, 61.
(52) Trætteberg, M.; Frantsen, E. B.; Mijlhoff, F. C.; Hoekstra, A. *J. Mol. Struct.* **1975**, *26*, 57.
(53) Trætteberg, M.; Frantsen, E. B. *J. Mol. Struct.* **1975**, *26*, 69.
(54) Firouzabadi, H.; Ghaderi, E. *Tetrahedron Lett.* **1978**, 839.
(55) Corey, E. J.; Suggs, J. W. *Tetrahedron Lett.* **1975**, 2647.
(56) Fuerstner, A.; Csuk, R.; Rohrer, C.; Weidmann, H. *J. Chem. Soc., Perkin Trans. 1* **1988**, 1729.
(57) Langkilde, F. W.; Wilbrandt, R.; Møller, S.; Brouwer, A. M.; Negri, F.; Orlandi, G. *J. Phys. Chem.* **1991**, *95*, 6884.
(58) Myers, A. B.; Li, B.; Ci, X. *J. Chem. Phys.* **1988**, *89*, 1876.
(59) Heinrich, G.; Blume, H.; Schulte-Frohlinde, D. *Tetrahedron Lett.* **1967**, *47*, 4693.
(60) Siebrand, W.; Zgierski, M. Z. In *Excited States*; Lim, E. C., Ed.; Academic Press: New York, 1979; Vol. 4, p 1.
(61) Suzuki, T.; Mikami, N.; Ito, M. *J. Phys. Chem.* **1986**, *90*, 6431.
(62) Myers, A. B. *J. Phys. Chem.* **1991**, *95*, 1536.
(63) Clark, R. J. H.; Dines, T. J. *Chem. Phys. Lett.* **1981**, *79*, 321.
(64) In *Langes Handbook of Chemistry*; Dean, J. A., Ed.; McGraw-Hill: New York, 1979.
(65) Dyck, R. H.; McClure, D. S. *J. Chem. Phys.* **1962**, *36*, 2326.